行政院國家科學委員會專題研究計畫　成果報告

子計畫一：以風洞實驗為基礎的高層建築防風設計準則

計畫類別：整合型計畫
計畫編號：NSC91-2211-E-032-013-
執行期間：91 年 08 月 01 日至 92 年 07 月 31 日
執行單位：淡江大學土木工程學系

計畫主持人：鄭啟明

報告類型：精簡報告
報告附件：出席國際會議研究心得報告及發表論文
處理方式：本計畫可公開查詢

中　華　民　國 92 年 11 月 27 日

行政院國家科學委員會補助專題研究計畫成果報告

※※※※※※※※※※※※※※※※※※※※※※※※※

※ ※

※ **以風洞試驗為基礎的高層建築防風設計準則(1/3)** ※

※ ※

※※※※※※※※※※※※※※※※※※※※※※※※※

計畫類別：□個別型計畫　　■整合型計畫

計畫編號：NSC91－2211－E－032－013－

執行期間：91 年　8 月　1 日至 92 年　7 月 31 日

計畫主持人：鄭啟明

本成果報告包括以下應繳交之附件：

□赴國外出差或研習心得報告一份

□赴大陸地區出差或研習心得報告一份

■出席國際學術會議心得報告及發表之論文各二份

□國際合作研究計畫國外研究報告書一份

執行單位：淡江大學土木系

中　華　民　國　92 年　　11 月　　26 日

行政院國家科學委員會專題研究計畫成果報告

以風洞實驗為基礎的高層建築防風設計準則

A Wind Tunnel Data based Intermediate Wind Resistant Design Guide for Tall Buildings

計畫編號：NSC 91-2211-E-032-013
執行期限：91 年 8 月 1 日至 92 年 7 月 31 日

主持人：鄭啟明　淡江大學土木系
計畫參與人員：劉啟威、許智傑　淡江大學土木系

一、中文摘要

本計畫嘗試對不同幾何斷面之建築物模型，以風洞物理模擬試驗探討其風載重之變化。建築物風洞試驗模型依研究目的可分為兩大類，其一為測試不同幾何斷面形式對風載重之效應，其二為細微幾何外型變化對風載重之影響。風力載重之量測是在大氣邊界層風洞中，藉由力平衡儀分析而得。結合足夠的風洞試驗數據及適當之結構動力分析，可建立一個以風洞試驗為基礎之高層建築防風設計準則。

關鍵詞：風洞實驗、高層建築、防風設計

Abstract

Tall building models with various geometry shapes were tested in wind tunnel for their wind loads. The tested models can be categorized into two sets of wind tunnel studies. The first set is to study the wind load acting on buildings with different cross-sectional shapes. The second set of study emphasized on the effects of minor variations on building shape. The wind loads of building models were measured by high frequency force balance in the turbulent boundary layer flows. With sufficient wind tunnel data, then collaborating with proper structural dynamics procedure, a wind tunnel databased wind resistant design guide for tall buildings can then be built.

Keywords:Wind Tunnel Test, Report Style, Wind Resistance Design

二、前言

高層建築的風效應包括結構系統所受風力、帷幕牆之表面風壓、人員舒適性以及行人環境風場等等。對於高層建築而言，設計風載重大多是藉由繁複之風洞試驗求得。然而，對於風載重影響最大之建築物幾何形狀與結構系統形式，卻大多在風洞試驗執行之前便已決定且難以變更。目前的高層建築設計流程中，風力規範是用於初步設計階段。因為風力規範是根據矩形斷面建物之風載重數據分析而得，對於其他斷面形式或有遮蔽效應之建築物來說，會偏向過於保守。另一方面，對於超高建築或柔性結構系統，現有風力規範則低估了其風載重之強度。若是初步設計階段能有一定準確度之風載重資料可方便提供設計者使用，上述之困擾即可有效解決。本計畫之目標就是嘗試建立一個介於風力規範與風洞試驗間，以風洞試驗為基礎之高層建築防風設計準則。

高頻力平衡儀(high frequency force balance）技術自從 Tschanz 於 1982 年提出以來，已迅速成為大多數風洞實驗室之標準量測方式。因為其操作簡易之特性，許多研究人員也藉此方式研究建築物幾何外型在細微變動下，對於降低風載重之效應。（Miyashita et al 1993, Kawai 1998, Kikitsu & Okada 1999, Tamura & Miyagi 1999）。

以結構設計觀點而言，大多數之建築物多少都需考慮氣彈力現象。因此，結合高頻力平衡儀量測技術與適當之結構動力分析流程，可準確地推估結構基底風載重

以及其在建築物高度上之分佈情形。若能夠取得建築物在不同流場、不同幾何斷面以及不同風攻角下之實驗數據，並詳細推估不同變數下，其實驗結果間之相關性，即可建立可行之高層建築風載重設計準則。

三、實驗設置

風洞試驗於淡江大學之大氣邊界層風洞實驗室中進行，試驗斷面為 18.0m × 2.0m × 1.5m。所使用之流場包括模擬開放地形之 BL1 流場（α=0.15）及模擬都市地形之 BL2 流場（α=0.32），邊界層高度約在 120cm 附近。實驗資料以模型高度之風速做為正規化之因子。實驗阻塞比小於 5%，可忽略其效應。風洞內之雷諾數在 4×10^4 以上，大於雷諾數相似性模擬之最低臨界雷諾數 2.0×10^4。

實驗所使用的 30 多個模型可分為兩大類。第一類模型是用以分析不同斷面型式對風載重之影響，包括 4 種子類型：（i）改變長寬比之矩形斷面、（ii）多邊形、（iii）L 斷面、（iv）不規則斷面。這一類模型之高寬比均為 7，體積與正方斷面模型一致。第二類實驗是以正方斷面模型為基礎，共有 4 種幾何外型上之變化：（i）高寬比、（ii）削角比、（iii）不同起始退縮高度之退縮斷面、（iv）不同退縮比之退縮斷面。這組模型之體積與高寬比 5 之正方斷面模型一致。建築物模型所受之風力以高頻力平衡儀量測，每一風向角量測一組數據，風向角之間距為 22.5 度，共計 16 個風向角。

四、實驗結果

雖然實驗量測了 16 個風向角，但是一般建築物之最大風載重多發生於風向與建築物垂直的情形。加上對稱之幾何外型造成橫風向風力（平均值）及扭轉向風力（平均值與擾動值）在 0 度攻角有較小之值，因此本文僅討論順風向風力之平均值與擾動值，以及橫風向風力之擾動值。

1．紊流邊界層對風載重之影響

兩種流場下之實驗結果，以正規化之風力係數詳列於表 1 與表 2。數據顯示，開放地形流場（BL1）相較於都市地形流場（BL2），實驗模型有較高之平均拖曳力、較低之擾動拖曳力與較低之擾動昇力。BL1 流場較小的梯度風速與紊流強度特徵，理論上是會造成拖曳力有較高之平均值及較低之擾動值。一般之鈍體也因此形成強度較強且相關性佳的渦散現象，導致較高之擾動昇力。比較擾動昇力係數與昇力頻譜，可發現開放地形流場之模型昇力頻譜有較高之尖峰值，而都市地形則有較寬之頻寬。較寬之頻寬是導致模型於都市地形下有較大擾動昇力係數之主因。由此可知，當接近渦散效應之臨界風速，開放地形流場內之高層建築會有較大之橫風向動態反應。而風速較低時，則是都市地形流場內之建築物受渦散引起之振動較大。

2．建築物斷面形狀對風載重之效應

本小節討論 4 組建築物外型，計有矩形斷面、多邊形、L 斷面與不規則斷面。這部分模型之高度與斷面積皆相同。為了有相同之比較基準，風載重以相同之寬度與高度進行正規化。

表 1. 不同斷面形式之高層建築風力係數

Model	BL1(α=0.15)			BL2(α=0.32)		
	C_D	C'_D	C'_L	C_D	C'_D	C'_L
R1	1.79	0.141	0.099	1.77	0.339	0.114
R2	1.53	0.126	0.078	1.44	0.317	0.190
R3	1.38	0.136	0.152	1.20	0.264	0.219
R4	1.21	0.104	0.182	0.87	0.237	0.236
R5	0.79	0.090	0.223	0.64	0.155	0.233
R6	0.63	0.069	0.225	0.52	0.123	0.253
R7	0.40	0.059	0.168	0.35	0.085	0.296
P0	0.78	0.102	0.126	0.50	0.124	0.160
P3	1.67	0.131	0.098	1.77	0.322	0.239
P4	1.10	0.109	0.209	0.87	0.211	0.235
P5	0.59	0.046	0.099	0.60	0.110	0.196
P6	0.76	0.053	0.056	0.76	0.139	0.122
P8	0.83	0.078	0.074	0.74	0.167	0.129
L1	1.89	0.152	0.076	1.87	0.376	0.178
L2	1.74	0.144	0.116	1.67	0.337	0.263

L3	1.58	0.134	0.161	1.45	0.292	0.335
M1	1.21	0.091	0.065	1.15	0.225	0.146
M2	1.08	0.104	0.137	1.00	0.229	0.191
M3	1.22	0.096	0.178	1.08	0.241	0.242
M4	1.60	0.111	0.051	1.66	0.292	0.102

（i）矩形斷面（R 系列）：隨寬深比增加（B/D），因為迎風面面積增加及側風面面積減少，順風向風力變大而橫風向風力變小。如圖 3 所示，對於寬深比小於 1 之短斷面，昇力頻譜出現明顯之渦散尖峰值；對於寬深比大於 1 之長斷面，昇力頻譜因為再接觸現象而出現較寬之頻寬。

（ii）多邊形（P 系列）：本系列圓斷面之雷諾數位於次臨界雷諾數附近，風力係數之使用需加以注意。其他斷面中，三角形斷面有最大之順風向風力，正方形有最大之橫風向擾動風力，五邊形之風載重最小。對順風向而言，平均及擾動拖曳力係數反映了拖曳力之強度與順風向結構反應之大小。然而對於橫風向擾動昇力係數，則未必真實表現出該方向之結構動態反應。昇力頻譜指出方形斷面渦散現象之尖峰值遠大於其他斷面；圓形及三角形此種渦散尖峰值的強度較方形斷面小一個數量級；五邊形及六邊形斷面之頻譜則顯得平滑而無明顯之尖峰值出現；而八邊形斷面則又顯示窄頻之現象，頻譜尖峰值僅稍小於圓形與三角形斷面模型。

表 2. 斷面微小變化對風載重之影響

Model	BL1(α=0.15)			BL2(α=0.32)		
	$\widetilde{F}_D$	$\widetilde{F}'_D$	$\widetilde{F}'_L$	$\widetilde{F}_D$	$\widetilde{F}'_D$	$\widetilde{F}'_L$
S1	0.88	0.881	0.867	0.86	0.954	0.893
S2	1.00	1.000	1.000	1.000	1.000	1.000
S3	1.15	1.018	1.138	1.178	1.035	1.159
S4	1.19	1.027	1.046	1.023	1.061	1.065
C1	0.88	1.138	1.102	0.723	0.701	0.764
C2	0.66	0.917	0.770	0.660	0.636	0.671
C3	0.71	0.752	0.628	0.755	0.740	0.715
RH1	1.13	1.018	0.755	1.149	0.909	0.768
RH2	1.03	0.917	0.796	1.138	0.905	0.732
RH3	0.99	0.853	0.770	1.096	0.952	0.764
RH4	0.95	0.862	0.796	1.060	0.918	0.764
SR1	0.99	0.853	0.770	1.096	0.952	0.764
SR2	1.07	0.939	0.730	1.029	0.887	0.759
SR3	0.98	0.881	0.730	1.067	0.871	0.714

註：”~” 表示以model S2為因子之正規化風載重

（iii）L 形斷面（L 系列）：大致而言，本系列斷面之順風向與橫風向風力皆大於其他系列之斷面，但是其昇力頻譜之尖峰值卻不顯著。由此可知 L 形斷面出現渦散共振之機會不大。

（iv）不規則斷面（M 系列）：實驗結果顯示，弧形斷面模型之順風向風力最大，橫風向風力最小。其他斷面是由方形斷面修改而來，昇力頻譜有明顯之尖峰值。

3．斷面部分變形對風載重之影響

本小節討論 4 組建築物外型之變化：（i）高寬比，（ii）削角比，（iii）不同起始退縮高度之退縮斷面、（iv）不同退縮比之退縮斷面。所有斷面皆以方形為基本形式，其所量得之風力係以高寬比 5 方形斷面（S2）為正規化之因子。

由實驗結果發現，當高寬比自 4 增加到 7，模型上半部會進入流場較為平穩與高速之區域，使得順風向平均風力增加了 30%左右。而高寬比對於順風向擾動風力的影響就不顯著。建築物之削角可有效降低平均與擾動拖曳力。退縮斷面對風載重有兩種效應：（i）建築高度之增加使得結構上半部有較多之區域浸沒於平穩而高速之流場中；（ii）退縮斷面之不連續性減弱流場分離的強度。此二種效應使得平均拖曳力變化不大，擾動拖曳力差異在 15%以下。

改變建築物之高寬比及退縮斷面對昇力頻譜之影響有限，其仍保有與方形斷面相似之窄頻頻譜特徵。而斷面之削角改變卻會顯著影響昇力頻譜，使其尖峰值降低並增大其頻寬。

五、建築物設計風載重

本小節將利用前述之風力頻譜，實際估算實場建築物之設計風載重。此建築物假設為 200 公尺高，高寬比 7 之方形斷面；結構密度 200Kg/m³，結構阻尼 0.01，自然週期 5 秒；設計風速假設為 42.5m/s。因為台灣風力規範與美國 ANSI/ASCE 7-88

相似，因此本研究僅考慮順風向風載重。

在推估風載重於各樓層之分佈情形時，有下列幾項假設：（i）風速剖面為指數律形式；（ii）只考慮結構之線性基本振態；（iii）結構反應之最大值以陣風反應因子估計；（iv）建築物高度上之共振反應分布與結構慣性力成正比；（v）背景反應部分之分佈方式與平均風載重成正比。

計算結果顯示，不論是開闊地形或是都市地型，根據風洞試驗數據分析而得之建築物風載重，樓層上半部之風力皆大於風力規範所提供之數據。而在較不重要之下半部樓層，則恰好相反。這些差異一部分是因為風力規範乃根據點狀結構物之假設做推論，並不考慮結構之真正振態。為了更準確了解結構在高度上之風載重分佈，未來之風力規範應當採納線性振態，以更接近實際狀況。

六、結論

本研究是建立一個風載重資料庫的部分工作。目前已完成兩種流場、30 多種建築物模型風力載重量測。這些資料可分為兩大類：（i）包含 20 種斷面形式之核心資料庫；（ii）包括流場變化及部分幾何形式改變之輔助資料庫。這些資料架構出高層建築抗風設計之基礎，並且需要更多的數據來擴充此資料庫。目前正同時進行另一個與本計畫相關之專家系統的開發，藉著結合這兩個計畫之成果，便可建立一個以風洞試驗為基礎之高層建築防風設計準則，提供結構技師事務所、工程顧問公司等從事高層建築結構設計或審核之單位，有一定準確度之設計風載重參考來源。

七、重要參考文獻

Hayashida, H. & Iwasa, Y. 1990. Aerodynamics shape effects of tall building for vortex induced vibration. *Journal of Wind Engineering and Industrial Aerodynamics* (33): 237-242.

Kawai, H. 1998, Effect of corner modifications on aeroelastic instabilities of tall buildings. *Journal of Wind Engineering and Industrial Aerodynamics* (74-76): 719-729.

Kikitsu, H. & Okada, H. 1999. Open passage design of tall buildings for reducing aerodynamics response. *Wind Engineering into 21st Century*, Larsen, Larose & Livesey.

Miyashita, K. et al. 1993. Wind induced response of high-rise buildings: effects of corner cuts or openings in square buildings. *Journal of Wind Engineering and Industrial Aerodynamics* (50): 319-328.

Tamura, T. & Miyagi, T. 1999. The effect of turbulence on aerodynamic forces on a square cylinder with various corner shapes. *Journal of Wind Engineering and Industrial Aerodynamics* (83): 135-145.

Yip, D.Y.N. & Flay, R.G.J. 1995. A new force balance data analysis method for wind response predictions of tall buildings. *Journal of Wind Engineering and Industrial Aerodynamics* (54/55): 457-471.

Tschanz, T. 1982. Measurement of total dynamic loads using elastic models with high natural frequencies. *Proceedings, International Workshop on Wind Tunnel Modeling Criteria and Techniques in Civil Engineering Applications*: 296-312. Maryland USA.

The Second International Symposium on Advanced in Wind and Structures (AWAS'02)出席會議報告

時間： 2002/8/21　至　2002/8/23

地點：韓國釜山

參與會議人數：參與會議者 80 餘人，中華民國籍 3 人。

經過：

8 月 20 日由台北出發經漢城抵釜山。21~23 日參與 The Second International Symposium on Advances in Wind and Structures (AWAS'02) 論文涵蓋的領域包括： Wind climate; Civil engineering structures; Tall buildings; Low-rise buildings; Cladding and roofing; Bridges Aerodynamics; Computational wind engineering; Risk analysis and social impact; Bluff body aerodynamics; Wind Tunnel techniques; Industrial aerodynamics; Wind energy 等。22 日發表論文，題目為：Acrosswind Aerodynamic Damping of Rectangular Tall Buildings。會中並與 Chang-Koon Choi, Korea Advanced Institute of Science and Technology, Korea.Ming Gu, Tongji University, China.John Holmes, Monash University, Australia.Ahsan Kareem, University of Notre Dame, USA.Kenny C. S. Kwok, Hong Kong University of Science and Technology, Hong Kong.Giovanni Solari, University of Genoa, Italy.Yukio Tamura, Tokyo Polytechnic University, Japan.You Lin Xu, Hong kong Polytechnic University, Hong Kong. 等學者表達逾 2003 年 10~11 月在台北召開小型國際風工程研討會，並獲允諾參加。

報告撰寫人：淡江大學土木系鄭啟明

參加國際學術研討會報告

會議名稱：第十一屆國際風工程研討會

11th International Conference on Wind Engineering

會議地點：Lubbock, Texas, USA

會議時間：2003/6/2 ~ 2003/6/6

風工程界自 1963 年開始每四年召開一次，是風工程學界最為重要的學術研討會，本次會議由美國德州大學主辦，共有來自 37 個國家，358 人註冊參加，其中以學界人士居絕大多數。本屆研討會在四天會議期間，宣讀 220 篇學術論文(presentations)及 140 篇張貼論文(posters)。論文涵蓋的領域包括：Codes and regulations; Wind climate; Civil engineering structures; Tall buildings; Low-rise buildings; Cladding and roofing; Environmental aerodynamics; Bridges; Computational wind engineering; Risk analysis and social impact; Bluff body aerodynamics; Wind Tunnel techniques; Industrial aerodynamics; Wind energy 等。

筆者在本屆研討會中發表兩篇論文，分別是 6 月 4 日下午張貼之 Design windloads on tall buildings: a wind tunnel data based ecpert system approach（第一作者王人牧教授），以及 24 日上午宣讀 Insight of aeroelastic behaviors of tall buildings under the influence o ftorsional/lateral frequency ratio.。二篇論文的部分研究經費均來自國科會，在此再次表示謝意。6 月 3 日晚間代表台灣出席國際風工程學會（International Association for Wind Engineering）的 Steering Committee Meeting。會中正式通過 IAWE 的組織章程，並選出義大利的 Prof. Giovanni Solari 為首屆的 president of IAWE。並決定 2007 年的第 12 屆國際風工程研討會在澳洲舉行。

參加本次會議除了能更精準的掌握個人從事風工程相關研究領域的發展情況之外，整體風工程領域較重要的發展方向有以下幾點：(1) 計算風工程(Computational Wind Engineering) 是所有風工程研究機構不可忽視的研究領域，然而未來二十年內在風工程實務應用方面仍無法取代風洞實驗，或是取得同等重要的地位。(2) 國際風力規範會逐步的進行整合，未來可能會出現 2 3 個差異性不大的版本，可供不同地區制訂其風力規範時參考之用。(3) 風災損害的評估是多數風害嚴重地區急需加強的工作項目。(4)就風工程在土木工程的重要性而言，我國目前的研究人力與成果水準需要加強，尤為可慮的是，在本次會議中有大批新生代的中國大陸籍學者（博士生），完全沒有來自台灣的年輕學者。土木學門宜加強推動風工程研究，吸引國內學者參與以因應下一世代大型結構的出現。

6 月 6 日上午以觀察者身份參加 ISO 風工程規範小組會議，對於該小組運作有一初步認識。可惜因預定之航班行程，未能全程參與。

Acrosswind Aerodynamic Damping of Rectangular Tall Buildings

*Chii-Ming Cheng[1)] Yi-Chang Chiang[2)]

Department of Civil Engineering, Tamkang University, Taipei, Taiwan, ROC

ABSTRACT

The acrosswind behavior and aerodynamic damping of rectangular shaped tall buildings with various side ratio and mass-damping coefficient were studied through wind tunnel aeroelastic model tests. Experimental results show that, the long rectangular building shape, *B/D*=2.0, is an aerodynamic stable building cross section regardless of the flow conditions. For short rectangular building shape, *B/D*=0.4, 0.6, 1.0, negative acrosswind aerodynamic damping might occur as functions of side ratio and flow condition. For these potentially aerodynamic unstable shapes, the negative aerodynamic damping occurs when acrosswind motion exceeds certain thresholds. Data also suggests that a model's negative aerodynamic damping is related to the side face reattachment of the free shear layer.

INTRODUCTION

Motion induced force, in the form of aerodynamic damping, has long been recognized as an important factor in the estimation of tall buildings' acrosswind response. Matsumoto (1986) used data from aerodynamic and aeroelastic tests to show that, for rectangular cylinder with 4.0 aspect ratio and side ratio of 0.6 and 1.0, acrosswind vibration exhibited instability in a α=0.2 flow field. Hayashida et. al. (1992) showed that, for a square cylinder with aspect ratio equals to 7.5, the acrosswind motion has positive aerodynamic damping in a α=0.25 flow field. Vickery & Steckley (1993) showed that, with augment of aerodynamic damping, the acrosswind response can be accurately predicted for a *H/D*=13.3 square cylinder in a α=0.112 flow field. Marukawa et. al. (1996) studied the aerodynamic damping of rectangular shaped buildings in open terrain flow field, showed positive aerodynamic damping in the alongwind direction for all models, and negative aerodynamic damping in the acrosswind direction for slender buildings with small side ratio. Cheng et.al. (2001) studied aerodynamic damping of square shaped building with various mass-damping coefficient. All earlier

---

1) Professor

2) Graduate Assistant

research works pointed out the importance of aerodynamic damping on buildings' response. In this paper, authors used aeroelastic models to study the acrosswind vibration behavior of isolated rectangular cylinders with side ratio *B/D*= 0.4~2.0 in two boundary layer flows. Besides the aeroelastic model tests, the acrosswind responses were calculated using the wind force spectra obtained from pressure models. Aerodynamic damping was then calculated via inverse response approach.

EXPERIMENTAL SETUP

The aeroelastic tests were conducted in a $18.0m \times 2.0m \times 1.5m$ boundary layer wind tunnel at Tamkang University. Two sets of turbulent boundary layer flows, *BL*1 and *BL*2, were generated to represent flows over open and urban terrain, respectively. *BL*1, the open terrain flow field, has a $\alpha = 0.15$ mean velocity profile, with turbulent intensity varying from 20% near ground to 3% at gradient height. *BL*2, the urban terrain flow field, has a $\alpha = 0.32$ velocity gradient with turbulent intensity varying from 35% to 6%. The gradient height is 120cm $\pm$10cm for both flow fields. During model testing, velocity at model height, U_H, was taken as the normalization factor for the reduced velocity, $U_r = U_H / f_0 D$.

Rigid body, two-way base pivoted aeroelastic model system was used to allow the aeroelastic model to have two sway mode motions. Rectangular cylinders with side ratio, *B/D* = 0.4, 0.6, 1.0, 2.0, were used in this project. All models have the same aspect ratio, *H/D* = 7, and the same model height, *H* = 70 cm. Blockage ratio is kept at less than 5 %. Reynolds number was kept greater than 4×10^4 for most of the wind tunnel experiments. To study buildings' aeroelastic behavior, the following form of mass-damping coefficient, M_d, was used as the experimental controlling parameter,

$$M_d = \frac{\int_0^H m(z)\Phi^2(z)dz}{\int_0^H \Phi^2(z)dz} \frac{\xi}{\rho D^2} \quad (1)$$

In which $\Phi(z)$ is the linear mode shape and ξ is structural damping ratio. Structural density, ρ_s, varies from 150 *kg/m*^{3} to 300 *kg/m*^{3}. Structural damping ratio, ξ, varying from 0.4% to 6%, was provided by an oil damper device at base of the aeroelastic model. The mass-damping coefficient varies from 0.6 to 10. Wind load spectra, obtained from pressure model, were used for the prediction of model's responses. These force spectra were also used as the basis of aerodynamic damping evaluation scheme. The total damping of the vibration system consists of structural damping and aerodynamic damping: $\xi_T\,(total) = \xi_S\,(structure) + \xi_a\,(aerodynamic)$. At the beginning of this study, it is verified that, for building has small acrosswind response, i.e., negligible aerodynamic damping effect, the predicted response agrees well with measurement. Based on that, aerodynamic damping was then evaluated by the following inverse response approach for its reliability. First, the structural damping, ξ_s, of aeroelastic model was determined. Then the system's total damping, ξ_T, was obtained by adjusting it numerically so that the calculated response, which was based on the acrosswind force spectra, equaled to the measurement. The aerodynamic damping was taken as the difference of the two damping values.

ACROSSWIND RESPONSE

B/D = 0.4

Eight mass-damping coefficient cases on *B/D*=0.4 shape were studied and shown in Figure 1(a) and 2(a). In *BL*1 flow field, responses from all testing models show distinct peak values as the results of vortex resonance. The corresponding reduced velocity indicates that the Strouhal number decreases as the acrosswind response increases. Figure 3(a) shows that the acrosswind response of the *B/D*=0.4 model can be classified into two parts. For mass-damping coefficient, M_d, varying from 2.0 to 3.6, the measured peak response (response near critical wind speed) is greater than the predicted value. For mass-damping coefficient, M_d, varying from 3.9 to 6.9, the measured response is always less than the prediction. In the *BL*2 flow field, the shifting of Strouhal number at large response can also be observed as in the *BL*1. When M_d varying from 1.9 to 3.9, the measured peak response is greater than the prediction. For model with M_d in between 5.1 to 7.0, the measured response is always less than the prediction. At large value of M_d, due to the broader bandwidth of lift force spectrum, there is no peak value near critical wind speed for both measured and calculated responses. In the cases of smaller M_d, i.e., large acrosswind motion, the negative aerodynamic damping is introduced at the vicinity of critical wind speed, and consequently, the acrosswind response shows distinct peak value at critical wind speed. Based on both the measured response and the prediction, it may conclude that the threshold of negative aerodynamic damping of *B/D*=0.4 model is at $\sigma_Y / D \approx 0.015$.

B/D= 0.6

Seven mass-damping coefficient cases on *B/D*=0.6 shape were studied. Figure 1(b) shows the acrosswind R.M.S response in *BL*1 flow field. Although it has larger acrosswind response than the *B/D*=0.4 model, the *B/D*=0.6 model shows only slight shifting on Strouhal number. For mass-damping coefficient, M_d =2.8~5.2, the measured peak response is greater than the prediction. For model with mass-damping coefficient, M_d= 5.7 and 7.3, the measured acrosswind response is less than the prediction. In the *BL*2 flow field, when mass-damping coefficient, M_d=2.9~5.2, the measured peak response is greater than the prediction and when the mass-damping coefficient, M_d = 5.7 and 7.6, the measured response is less than the prediction. Similar to the *B/D*=0.4 model in *BL*2 flow field, there is only weak resonance at critical wind speed. The threshold of negative aerodynamic damping of B/D=0.6 model is $\sigma_Y / D \approx 0.02$.

B/D= 1.0

In flow field *BL*1, acrosswind response of the *B/D*=1.0 model can be classified into three regions of building's mass-damping coefficient.

(1) Aerodynamic stable region, $M_d \geq 6.28$. In this region, building's motion induced insignificant aeroelastic effect, mostly positive aerodynamic damping.
(2) Aerodynamic unstable region, $5.82 \geq M_d \geq 2.76$. In this region, negative aerodynamic damping occurs. For reduced velocity less than 8.0, the predicted responses agree well with measurements. When U_r > 8.0, motion induced force starts to emerge, i.e., measured values become greater. This negative aerodynamic damping effect is strongest near critical velocity. As wind speed exceeds critical value, aeroelastic effect weakens and response of aeroelastic model gradually approaches predicted value.
(3) Aerodynamic divergence region, $M_d \leq 2.18$. In this region, The acrosswind response amplitude is about an order greater than the other two regions, once building's acrosswind response amplified due to the vortex induced instability, galloping is likely to occur and

structural response divergent with wind speed.

Data also shows that σ_y / D =3% is the negative aerodynamic damping threshold for the square building in open terrain flow field. The responses measured in *BL*2 indicate that, regardless of buildings' mass-damping coefficient, acrosswind response has no peak value at critical wind speed. Even when acrosswind response well exceeds the aeroelastic threshold, σ_y/D>3%, presence of high turbulence would damp the aeroelastic effect, i.e., negative aerodynamic damping will not occur in *BL*2 flow field.

B/D = 2.0

Based on the lift force spectra, it is clearly shown that, for *B/D*= 2.0, the vortex shedding process is considerably affected by the reattachment phenomenon. Instead of the narrow-band feature as in the cases of $B/D \le 1.0$, the lift force spectra become more of the broadband nature. Negative aerodynamic damping is not expected in this case, therefore, only two cases of mass-damping coefficient were studied, M_d = 3.5 and 6.4, respectively. Figure 1(d) and 2(d) indicate that, for the flow field and mass-damping coefficient cases in this study, the acrosswind response of model *B/D*=2.0 has no vortex shedding resonance. The acrosswind response simply increases with wind speed. Except a little positive aerodynamic damping effect at wind speed greater than the critical, the predicted response agrees quite well with measurement.

AERODYNAMIC DAMPING

Figure 6 and 7 show the aerodynamic damping of models with *B/D*=0.4, 0.6 and 1.0. Except for the *B/D*=1.0 model in the urban terrain flow field, negative aerodynamic damping clearly is a function of reduced velocity. In the open terrain flow field, *BL1*, all three models exhibit "lowest" negative aerodynamic damping near critical wind speed: $U_{r,cr} \approx$ 9.0, 9.5 and 11.0 for *B/D*=0.4, 0.6 and 1.0, respectively. The mass-damping coefficient, which combines two different effects, does not show clear effect on the magnitude of aerodynamic damping. However, it seems that models with lower value of mass-damping coefficient tend to have wider velocity range of negative aerodynamic damping effect. At the vicinity of critical wind speed, *B/D*=0.4 has aerodynamic damping at ξ_{aero}=-0.018~-0.022, *B/D*=0.6 model has the lowest aerodynamic damping among three models at ξ_{aero}=-0.02~-0.03, while the *B/D*=1.0 model has aerodynamic damping at ξ_{aero}=-0.015~-0.018. As for the *B/D*=0.4 and 0.6 models in the urban terrain flow field, the negative aerodynamic damping still shows the lowest value at critical wind speed, but has a broader velocity range than models in the open terrain flow field. The *B/D*=0.4 model has aerodynamic damping about ξ_{aero}=-0.014~-0.025 at $U_{r,cr} \approx 9.0$, and the aerodynamic damping of *B/D*=0.6 model shows ξ_{aero}=-0.02~-0.025 at $U_{r,cr} \approx 9.5$. Considering the aerodynamic damping and the lift force spectra of the rectangular models, it seems that the side ratio and free stream turbulence cast similar effect on the aerodynamic damping as the way they affect the vortex shedding process and the lift force spectra. In the cases of *B/D*=0.4 and 0.6 in *BL*1, the free shear layer is subjected to little or no interference from the rear corner of the cylinder, therefore, increasing the free stream turbulence will broaden the spectral bandwidth of the lift force but does not weaken the vortex formation and the shedding process. The spectral peak of the lift force spectra in *BL*2 is about the same or even higher than in *BL*1. Similarly, in these cases, the negative aerodynamic damping occurs over a wider velocity range in *BL*2, but shows little difference in its magnitude. On the other hand, for the square cylinder, the lift force is significantly weakened by high turbulence in *BL*2, and at the same time the negative

aerodynamic damping no longer exists. In other words, a model's negative aerodynamic damping is closely related to whether or not the cross sectional shape and the oncoming turbulence will weaken the vortex intensity and consequently the lift force. Or, it can be said that the existence of a model's negative aerodynamic damping is strongly related to the nature of reattachment of the model. It should be noticed that only four cross sectional shapes are used in the present study, more data is needed to verify this observation.

CONCLUSIONS

Some of the conclusions from this research are:

(1) B/*D*=2.0 is an aerodynamic stable shape for tall buildings. Negative aerodynamic damping effect doest not occur for this cross sectional shaped buildings. *B/D*=1.0 model is stable in urban terrain flow field, but has negative aerodynamic damping in open terrain flow field when mass-damping coefficient, $M_d \leq 5.82$. For small side ratio building shape, *B/D*=0.4 and 0.6, the negative aerodynamic damping will occur, regardless of the flow field, when the mass-damping coefficient becomes less than 4.0 and 5.0, respectively.

(2) The thresholds for the negative acrosswind aerodynamic damping effect are σ_y / D=1.5%, 2.0% and 3.0% for *B/D*=0.4, 0.6 and 1.0, respectively. Exceeding it, motion induced force becomes significant; response calculated based on lift force spectra will be underestimated.

(3) Data suggests that a model's negative aerodynamic damping is strongly related to the nature of reattachment of the model. More data is needed to verify this observation.

REFERENCES

Cheng, C.M., Lu, P.C., Tsai, M.S., (2001), "Acrosswind Aerodynamic Damping of Isolated Square Shaped Buildings", *Proceedings of the Fifth Asia-Pacific Conference on Wind Engineering*, Kyoto/Japan.

Hayashida, H., Mataki, Y., Iwasa, Y., (1992), "Aerodynamic damping effects of tall building for a vortex induced vibration", *Journal of Wind Engineering and Industrial Aerodynamics*, 41-44, 1973-1983.

Matsumoto, T., (1986), 'On the Acrosswind Oscillation of Tall Buildings', *Journal of Wind Engineering and Industrial Aerodynamics*, 24, 69-85.

Marukawa, H., Kato, N., Fujii, K., Tamura, Y., (1996), "Experimental evaluation of aerodynamic damping of tall buildings", *Journal of Wind Engineering and Industrial Aerodynamics*, 59, 177-190.

Vickery, B.J., Steckley, A., (1993), "Aerodynamic Damping and Vortex Excitation on an Oscillating Prism In Turbulent Shear Flow", *Journal of Wind Engineering and Industrial Aerodynamics*, 49, 121-140.

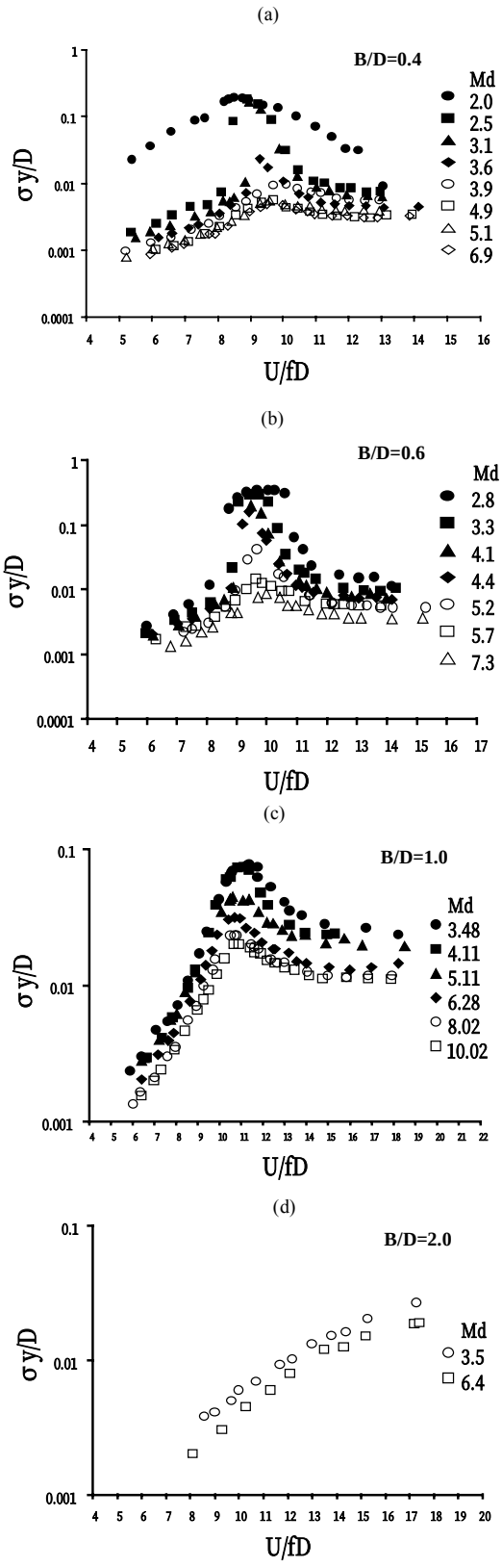

Fig1. R.M.S. acrosswind response in BL1.

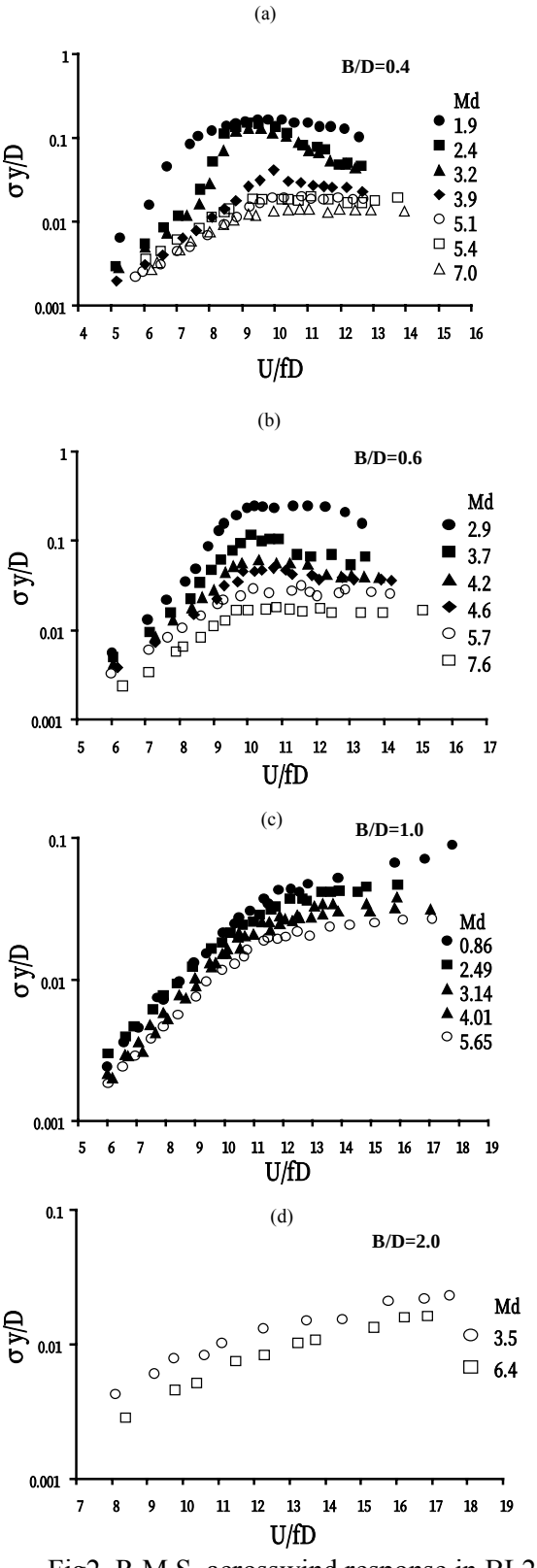

Fig2. R.M.S. acrosswind response in BL2

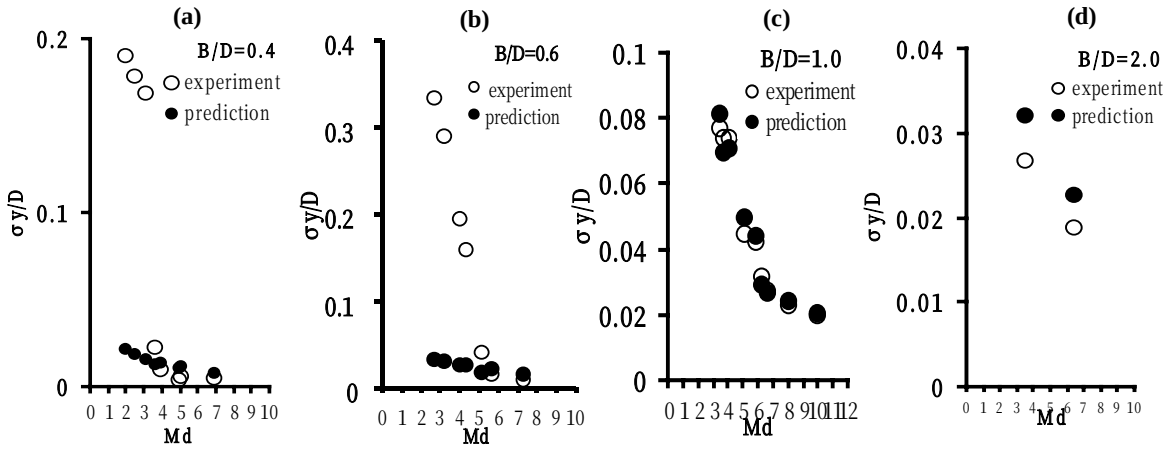

Fig3. Comparisons of peak acrosswind response in BL1.

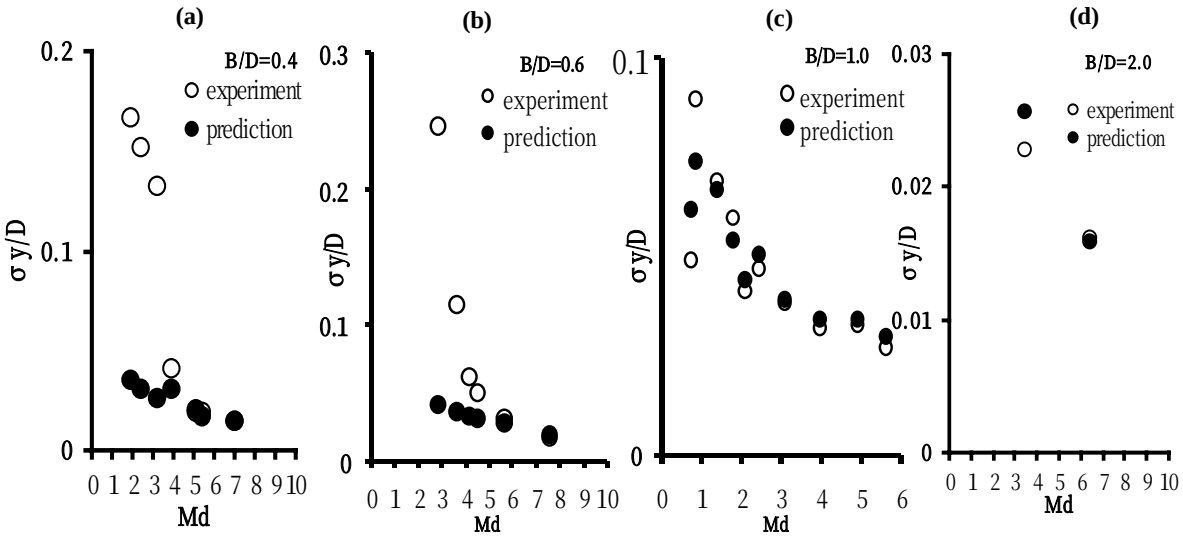

Fig4. Comparisons of peak acrosswind response in BL2.

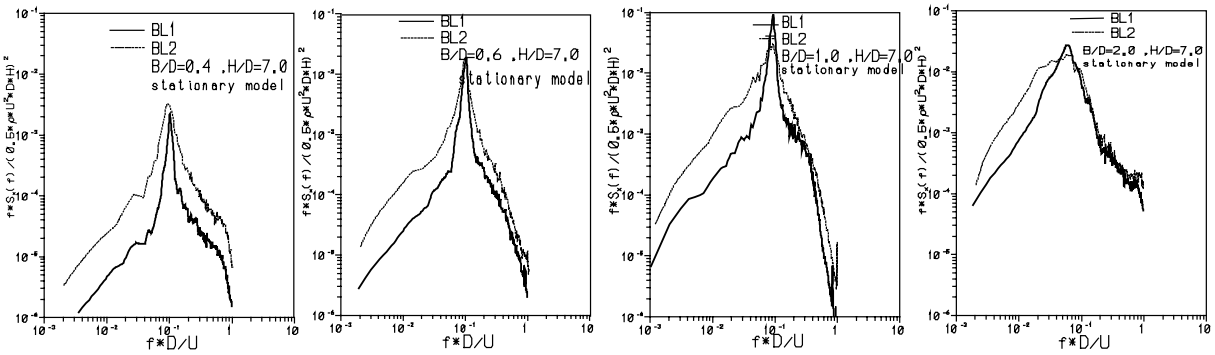

Fig5. Acrosswind generalized force spectra of rectangular shaped buildings

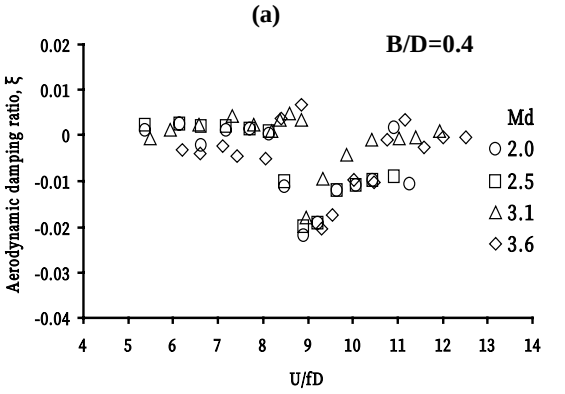

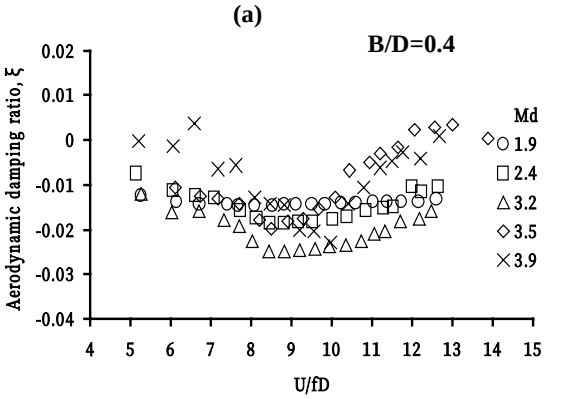

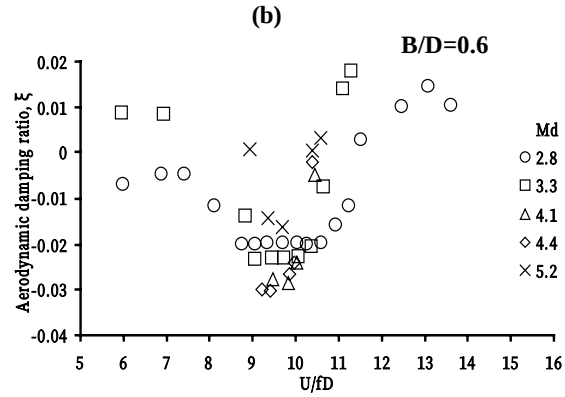

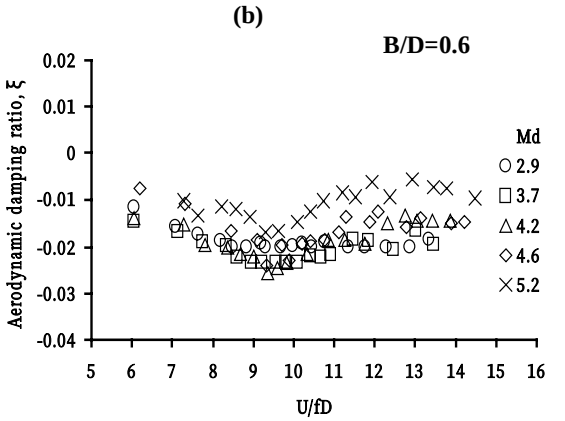

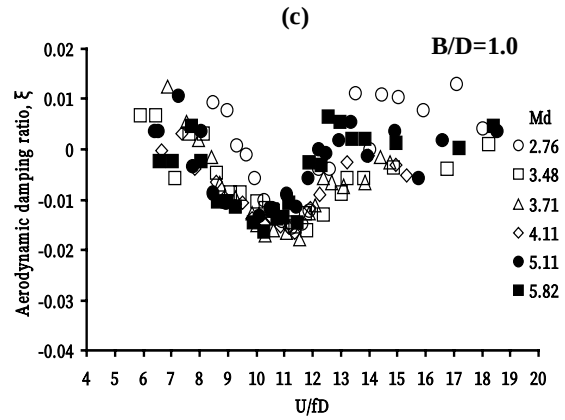

Fig6. Acrosswind aerodynamic damping for models in BL1

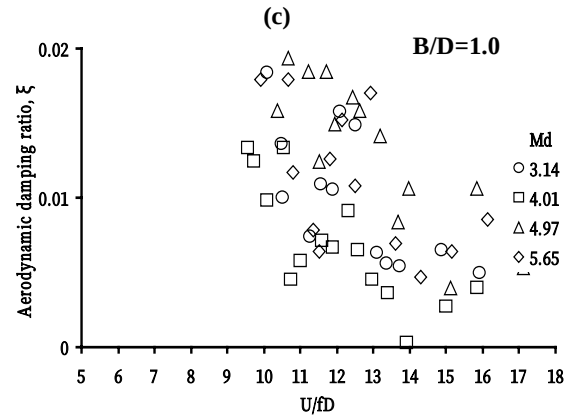

Fig7. Acrosswind aerodynamic damping for models in BL2

Insight of aeroelastic behaviors of tall buildings under the influence of torsional/lateral frequency ratio

Chii-Ming Cheng[a], Zheng-Xun Lin[a], Ming-Shu Tsai [a]

[a]*Department of Civil Engineering, Tamkang University, Taipei, Taiwan, ROC*

ABSTRACT: Rigid square pressure models mounted on base pivoted spring-damping system were used to study the aeroelastic behaviors of tall buildings. During wind tunnel experiments, data of the 28 pressure taps were simultaneously sampled along with buildings' motion and wake velocity measurements. It was found that the ratio of buildings' torsional natural frequency to the lateral frequency, R_f, plays a governing role on buildings' vibration mode. When the frequency ratio, R_f, approaches but greater than 1.0, coupled vibration mode will interfere the vortex shedding process and the buildings' dynamic response reduces significantly. For R_f less than 1.0, the vortex shedding process will be enhanced by building's motion, consequently, buildings' dynamic response steadily increases.

KEYWORDS: tall buildings, aeroelastic, frequency ratio, wind tunnel

InTRODUCTION

For a tall building with slender geometry shape and flexible structural system, the self-excited force due to excessive motion is a wind engineering phenomenon needs to be tackled with care. Marukawa et al. [1], Cheng et al. [2] and others have studied the motion induced aerodynamic damping by means of aeroelastic model tests. Vickery & Steckley [3], Chen et al. [4], Katagiri et al. [5] used force oscillation approach to investigate the characteristics of motion-induced force. For tall buildings with either similar natural frequencies or mass-stiffness eccentricity, Kareem [6], Safak & Foutch [7] studied the lateral/torsional coupling effect under wind loads through semi-analytical models. Their studies indicated that when the torsional/lateral frequency ratio is close to 1.0, the presence of mass-resistance eccentricity may cause mode-coupling effects, and increase the building's dynamic response significantly. Xu et al. [8], Cheng et al. [9], Katagiri et al. [10], Thepmongkorn & Kwok [11] conducted aeroelastic tests to studied the effects of eccentricity on buildings' mode-coupled oscillation under wind loads. The results showed buildings' behavior deviates from the analytical analysis. In other words, the tall building's mode-coupled vibration is an aeroelastic phenomenon needed to be investigated through aeroelastic approach.

In the present study, an aeroelastic pressure model was built to investigate tall buildings' mode-coupled aeroelastic behaviors under the actions of wind loads. There are two important factors that could cast significant influence on this subject, namely, the torsional/lateral frequency ratio and mass-stiffness eccentricity. Only the torsional/lateral frequency ratio was studdied in this article. By controlling the lateral/torsional natural frequency ratio, the surface pressure and wind loads were measured at a variety of coupled mode vibrations. In this approach, researchers could have a better understanding on the nature of the wind pressure and wind loads at various oscillatory conditions. A torsional/lateral coupled structural model was used to further explain the cause of the observed aeroelastic behaviors of tall buildings.

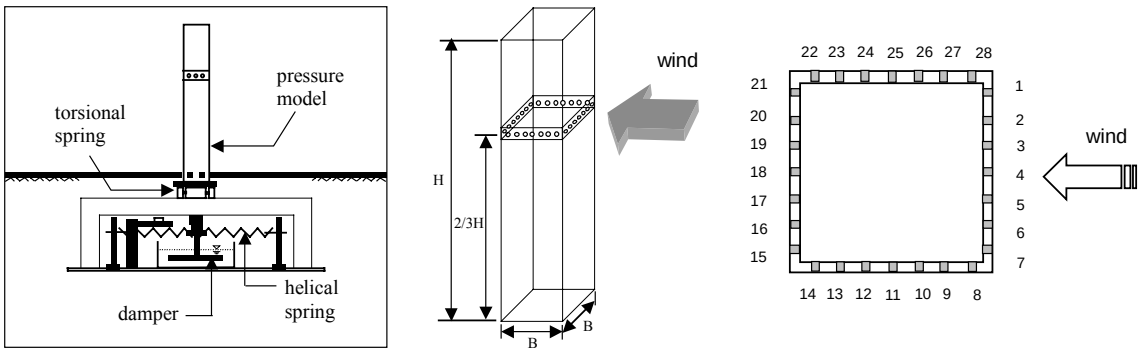

Figure 1. Schematics of aeroelastic pressure model.

Experimental Apparatus

The aeroelastic pressure model tests were conducted at the Boundary Layer Wind Tunnel II, Tamkang University. BLWT II is an open circuit, suction type wind tunnel, has a $18.0m \times 2.0m \times 1.5m$ test section. A turbulence boundary layer representing the flows over open terrain was used in this study. It has a $\alpha = 0.15$ mean velocity profile, with turbulent intensity varying from 20% near ground to 3% at the gradient height. The gradient height is 120cm $\pm$ 10cm.

In order to investigate the insight of the wind-structural interactions, a new type of pressure model was built. The so-called aeroelastic pressure model is consisted of a rigid square cylinder mounted on a base pivoted spring-damping system, as shown in Figure 1. A square cylinder with a width of 10 cm, height 70 cm, and aspect ratio H/D = 7 was chosen to represent the high-rise building. The pressure model was instrumented by 28 pressure taps uniformly distributed on the two-third of building height, $\frac{2}{3}H$. During wind tunnel experiment, the wind pressure data of the 28 pressure taps were simultaneously sampled along with buildings' motion and wake velocity measurements. The tri-axial mechanism at base provides alongwind, acrosswind and torsional motions. It was found that the ratio of buildings' torsional natural frequency to the lateral frequency plays a dominate role on buildings' vibration mode, consequently, it determines the acrosswind load and the wind induced vibration of tall buildings. The frequency ratio, R_f , is defined as: R_f = torsional frequency/lateral frequency. Total of 7 cases of R_f were used during this study, R_f = 2.0, 1.4, 1.1, 1.05, 0.95, 0.9, 0.8. Most of the building models have structural density of $\rho_s = 200kg/m^3$ and 2.2% of critical damping, which corresponds to mass-damping coefficient, M_D= 3.93. At this mass-damping coefficient, the square shaped building tends to have negative acrosswind aerodynamic damping in the chosen flow field. Another model with 3.5% of critical damping (M_D= 6.25) was used for comparison only. The blockage ratio was less than 5%; therefore, this effect was ignored. The Reynolds number was kept greater than 4×10^4 for most wind tunnel experiments.

Experimental Results

Buildings' responses

At the beginning of this study, the structural response of models with two different mass-damping coefficient, M_D= 3.93 & 6.25, were compared with the predictions based upon the wind loads acting on a stationary model. The frequency ratio, R_f, was set up at 2.0, so that the mode coupling effect was excluded. The mean and dynamic alongwind responses, shown in Figure 2, agree quite well with the predicted value. As for the acrosswind dynamic response, when the RMS response is small, i.e., $\sigma_y \le 0.03D$, the acrosswind response of M_D=6.25 model is equal or slightly less than the predicted response. For model with mass-damping coefficient M_D= 3.93, the acrosswind RMS response is well exceeding the 0.03D threshold, measured dynamic response become significantly greater than the predicted value due to the effect of negative aerodynamic damping.

Figure 3 shows the alongwind acrosswind and torsional RMS response of testing models. Comparing to the case of R_f = 2.0, it clearly indicates that when the frequency ratio, R_f, approaches but greater than 1.0, the models' acrosswind response reduces significantly. In the case of R_f = 1.1 & 1.05, the acrosswind responses are not only less then the R_f = 2.0 model but also notably less than the prediction based upon wind load of a stationary model. However, in the cases of R_f less than 1.0, the testing models graduatly drift into a state of aerodynamically instablility, their acrosswind responses increase and would well exceed the response of R_f = 2.0. These models also exhibit considerable increase on the alongwind and torsional dynamic responses when R_f becomes less than 1.0. The dynamic responses of the R_f =0.8 & 0.9 model are almost one order of magnitude greater then the R_f = 1.1 & 1.05 models. In short, R_f =1.0 is a critical value of the torsional/lateral frequency ratio. The square shaped tall buildings would register contrary aeroelastic characteristics when its frequency ratio falls at the opposite side of 1.0.

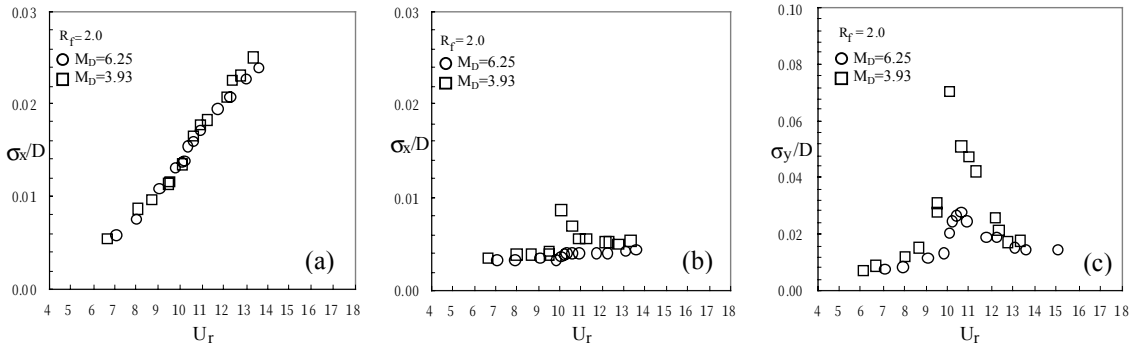

Figure 2. Effects of mass-damping coefficient on building's response. (a) alongwind (mean) (b) alongwind (R.M.S.) (c) acrosswind (R.M.S.)

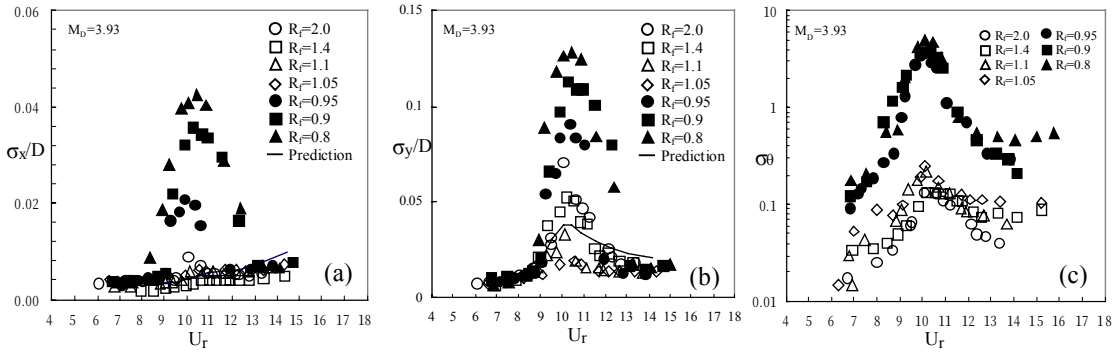

Figure 3. Building's R.M.S. response at various frequency ratio.(a) alongwind (b) acrosswind (c) torsional

Wind loads

The RMS lift force coefficients of models with M_D= 3.93 and frequency ratio R_f = 2.0, 1.1, 0.9, are shown in Figure 4. For R_f = 2.0, i.e., without the torsional/lateral coupling effect, the non-dimensional RMS lift force measured from the aeroelastic pressure model is slightly less than the stationary model except at critical wind speed. However, in the case of R_f close but greater than 1.0, the lift coefficient becomes less than the stationary model even at critical

wind speed; on the other hand, when R_f becomes less than 1.0, the lift coefficient shows significant increase near critical wind speed. Similar results can be observed on the torsional force measurement and the velocity spectra measured at the wake of building model.

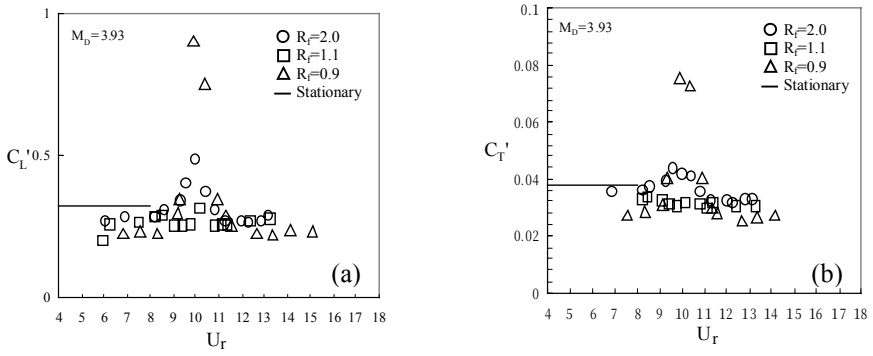

Figure 4. Wind force coefficients at various frequency ratio. (a) R.M.S.-lift (b) R.M.S.-torque

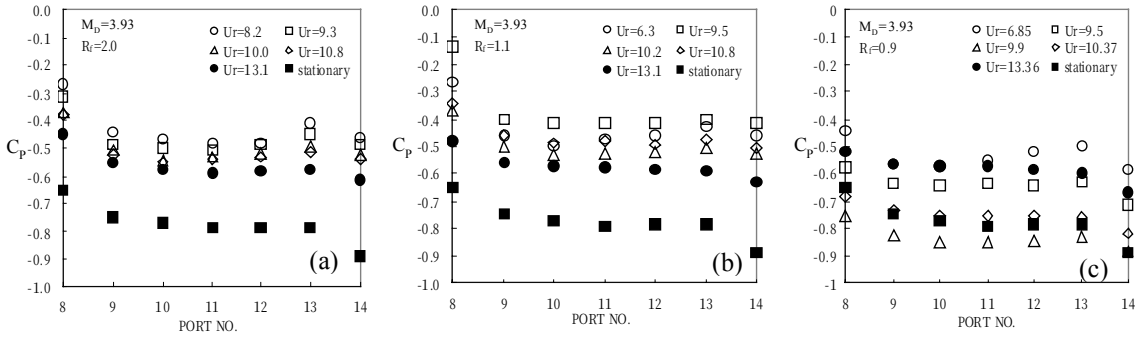

Figure 5. Distributions of mean pressure coefficients on model side face. (a) $R_f = 2.0$ (b) $R_f = 1.1$ (c) $R_f = 0.9$

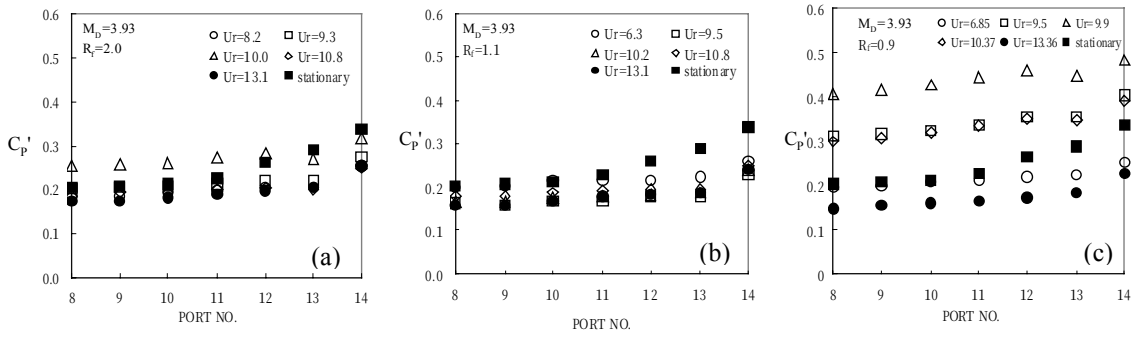

Figure 6. Distributions of R.M.S. pressure coefficients on model side face. (a) $R_f = 2.0$ (b) $R_f = 1.1$ (c) $R_f = 0.9$

Figure 5(a)~5(c) show the side face mean pressure distribution of models at various wind speed. It can be observed that, for model with frequency ratio R_f = 2.0 & 1.1, the surface pressure taken from the oscillatory model is consistently greater than the stationary model for all pressure ports, and show some pressure recovery near the rear corner. Between the two models, the R_f = 1.1 model exhibits higher surface pressure than the R_f = 2.0 model. When the frequency ratio becomes less than 1.0, the R_f = 0.9 model has the lowest side face pressure among the three oscillating models. Near critical wind speed, $U_r \approx 10.0$, the R_f = 0.9 model exhibits equal or lower pressure than the stationary model. The side face RMS pressure

coefficients are shown in Figure 6(a)~6(c). Models with frequency ratio R_f = 2.0 & 1.1, show similar or slightly lower value of C'_P than the stationary model. The R_f = 0.9 model, on the other hand, shows significant increase of C'_P near critical wind speed. The base pressure coefficients, $\overline{C}_{Pb}$ & C'_{Pb}, have the similar trend. For models with frequency ratio greater than 1, R_f = 2.0 & 1.1, the mean base pressure taken from the oscillatory models is greater, and the RMS base pressure is slightly lower than the stationary model. For models with frequency ratio less than 1, R_f = 0.9, the oscillatory model has lower mean base pressure and higher RMS base pressure near critical wind speed.

A single hot film sensor, placed at 1.0 D from the leeward face and 1.5 D from the model's centerline, was used to measure the wake velocity fluctuations as an indication of vortices intensity. For frequency ratio equals to 2.0, the spectral peak gradually increases with wind speed and reaches maximum value at critical wind speed. When the frequency ratio equals to 1.1, the maximum of the spectral peak decreases and the largest spectral peak can be observed when frequency ratio equals to 0.9.

Effects of vibration modes

The cross-correlation coefficients between acrosswind motion and torsional motion, $R_{y\theta}(0)$, are shown in Figure 7. When R_f = 2.0 & 1.1, the cross-correlation coefficients equal to 1.0, $R_{y\theta}(0) \approx 1.0$, which suggests a nearly perfect correlation between the two vibration modes. In other words, the building has maximum counter clockwise twist angle coincide with maximum across wind motion. For R_f = 0.9, however, the cross-correlation has an 180^o phase angle shift and shows coefficient equals to -1.0, $R_{y\theta}(0) \approx -1.0$, which suggests maximum clockwise twist angle coincide with maximum across wind motion. Based on this information and the coordinate system of wind tunnel tests, the two distinct vibration modes can be depicted as shown in Figure 8. The first vibration mode, which occurs near critical wind speed and frequency ratio greater than 1.0, has the center of gyration locates at upstream of the model. Under such an oscillating

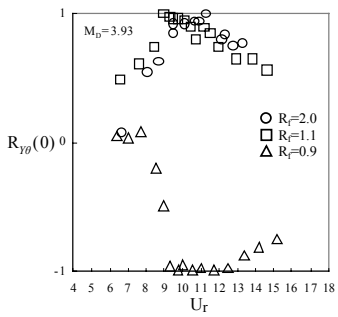

Figure 7. Correlations between model's torsional & lateral motions.

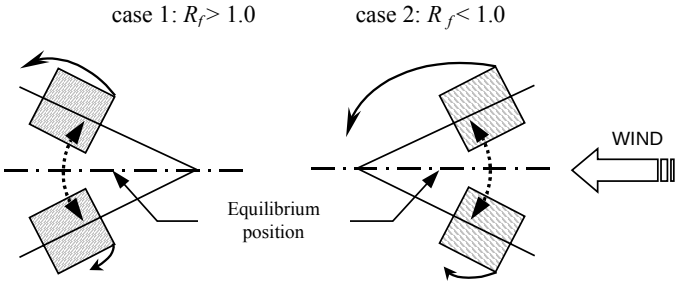

Figure 8. Observed vibration modes under various frequency ratio.

mode, the building's rear corner is more likely to interfere with the separated free shear layer, weaken the wake vortices, cause the increase of the side face pressure and base pressure, and hence stabilize the acrosswind motion. When the frequency ratio becomes less than 1, the building has its center of gyration at downstream, then, the vortex shedding process is likely to be enhanced by the model's oscillation, the side face and base pressure become more negative than the stationary model, and consequently increase the amplitude of acrosswind vibration.

Mode coupling between lateral and torsional vibration

In order to explain the observed aeroelastic behavior, it is necessary to look into building's structural dynamic characteristics. Consider an acrosswind and torsional axes weakly coupled structural system with coordinate system shown in Figure 9. The undamped equation of motion can be written in the following form:

$$\begin{bmatrix} m & 0 \\ 0 & m \end{bmatrix} \begin{Bmatrix} \ddot{y} \\ r\ddot{\theta} \end{Bmatrix} + \begin{bmatrix} k_y & \varepsilon k_y \\ \varepsilon k_y & k_\theta^* \end{bmatrix} \begin{Bmatrix} y \\ r\theta \end{Bmatrix} = \begin{Bmatrix} F_y \\ \frac{1}{r}\tilde{M}_\theta \end{Bmatrix} \tag{1}$$

In which, $r = \sqrt{I/A}$ is the radius of gyration; $k_\theta^* = k_\theta / r^2$, where k_θ is torsional stiffness; $\varepsilon = \varepsilon_x / r$ is a non-dimensional eccentricity. Let $\omega_\theta = a\omega_y$, where $\omega_\theta = \left(k_\theta / mr^2\right)^{1/2}$ is the natural frequency of torsional mode, and $\omega_y = \left(k_y / m\right)^{1/2}$ is the natural frequency of acrosswind axis. It can be derived that there exist two coupled vibration modes. The natural frequencies and corresponding mode shapes are as follows,

(i) First mode

$$\omega_1^2 = \frac{1}{2}\left[1 + a^2 - \sqrt{\left(1-a^2\right)^2 + 4\varepsilon^2}\right]\omega_y^2 \;;\left(\frac{Y}{r\Theta}\right)_1 = \frac{2\varepsilon}{1 - a^2 + \sqrt{(1-a^2)^2 + 4\varepsilon^2}} \tag{2}$$

$$a \to 1.0; \quad \omega_1 \approx \omega_y\sqrt{1-\varepsilon}; \quad \left(\frac{Y}{r\Theta}\right)_1 \approx 1 \tag{3}$$

(ii) Second mode

$$\omega_2^2 = \frac{1}{2}\left[1 + a^2 + \sqrt{\left(1-a^2\right)^2 + 4\varepsilon^2}\right]\omega_y^2 \;;\; \left(\frac{Y}{r\Theta}\right)_2 = \frac{2\varepsilon}{1 - a^2 - \sqrt{(1-a^2)^2 + 4\varepsilon^2}} \tag{4}$$

$$a \to 1.0; \quad \omega_2 \approx \omega_y\sqrt{1+\varepsilon}; \quad \left(\frac{Y}{r\Theta}\right)_2 \approx -1 \tag{5}$$

The natural frequencies and mode shapes of a square shaped building with eccentricity $\varepsilon_x = 0.05B$ and various frequency ratios are listed in Table 1, in which M_θ & M_y are the mode generalized mass contributed from θ and *y* coordinate, respectively. By using the ratio of generalized mass, $\left(M_y / M_\theta\right)_i$, as an indicator, the predominant motion of each mode can be determined. When the frequency ratio approaches 1.0 from the left hand side, i.e., $a > 1.0$, $\omega_\theta > \omega_y$, Table 1 shows that the first mode with its frequency lower than the uncoupled lateral frequency, i.e., $\omega_1 < \omega_y$, has M_y significantly greater than M_θ. Therefore, it is a lateral motion predominant mode. The second mode with frequency higher than the uncoupled case, on the other hand, has M_θ much greater than M_y, is thus a torsional predominant mode. When the frequency ratio approaches 1.0 from the right hand side, i.e., $a < 1.0$, $\omega_\theta < \omega_y$, the first mode becomes torsional predominant and the second mode lateral motion predominant. The mode shapes of the two opposite coupled modes are plotted in Figure 10.

Comparing with the wind tunnel measurement, it seems to suggest that when $R_f > 1.0$ ($\omega_\theta > \omega_y$), the second mode will be suppressed and tall buildings' motion will be dominated by the first mode (the lateral mode). On the other hand, when the frequency ratio becomes less than one, i.e., $R_f < 1.0$ ($\omega_\theta < \omega_y$), the first mode will be suppressed and the second mode will prevail (again, the lateral mode). Earlier study indicates that the acrosswind motion casts much stronger influence on square buildings' negative aerodynamic damping than the pure torsional motion. The present experimental data also show that the lateral mode contributes to the corner's acrosswind response 3 to 60 times more the torsional mode. This is probably the primary reason of the lateral dominance of the mode-coupling aeroelasticity.

The wind tunnel experimental data and the aforementioned dyanmic analysis lead to the following statements. The wind induced vibration of a torsional/lateral coupled tall building is an complex aeroelastic phenomenon. Between the two coupled structural modes, the wind-structure interaction mechanism would always select the lateral predominant mode and suppress the other mode. However, it is to be noted that, only the the effect of frequency ratio is studied in the present investigation, the aeroelastic behavior of tall buildings with eccentricity needed to be examed.

Table 1.Frequencies and mode shape under beat phenomenon

	$\omega_\theta > \omega_y$				$\omega_\theta = \omega_y$		$\omega_\theta < \omega_y$		
a	1.4	1.2	1.1	1.05	1.0	0.95	0.9	0.8	0.6
ω_1 / ω_y	0.970	0.940	0.902	0.871	0.827	0.771	0.707	0.570	0.316
ω_2 / ω_y	1.990	1.500	1.308	1.232	1.173	1.131	1.103	1.070	1.044
$(M_y / M_\theta)_1$	32.7	8.33	3.15	1.79	1.000	0.574	0.351	0.162	0.064
$(M_y / M_\theta)_2$	0.031	0.120	0.317	0.558	1.000	1.743	2.853	6.158	15.59

Assume $\varepsilon_x = 0.05b$, $\varepsilon = \varepsilon_x / r = 0.17$, $\omega_\theta = a \cdot \omega_y$

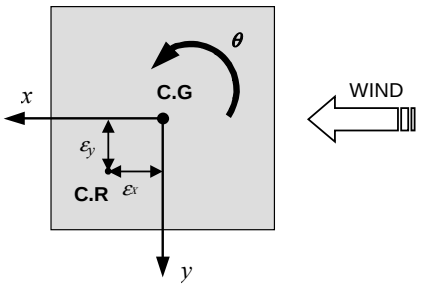

Figure 9. Coordinate system for wind tunnel test and analytical model.

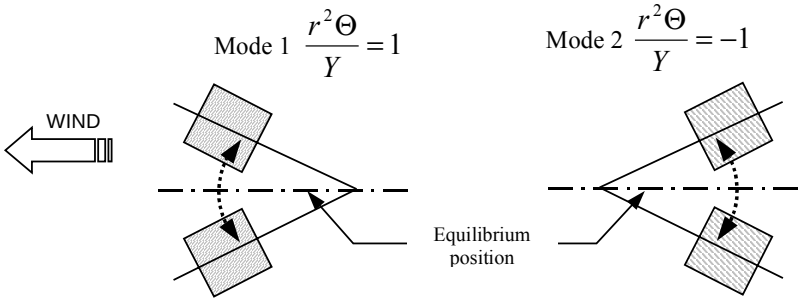

Figure 10. Torsional / lateral coupled structural mode shape at $\omega_\theta = \omega_y$.

Conclusions

A few statements can be concluded based on this investigation:

(1) When buildings' torsional/lateral frequency ratio close to 1, it becomes an important parameter that dominants the aeroelastic behavior of tall building.

(2) When torsional/lateral frequency ratio greater than 1.0, $R_f > 1.0$, the model vibrates with

center of gyration located at upstream of the model, the separated free shear layer is interfered by buildings' rear corner, wake vortices weaken, lift force decreses and the acrosswind motion stabilized. When $R_f < 1.0$, the center of gyration is at downstream, the vortex shedding process is likely to be enhanced, lift force increases, and acrosswind vibration amplified.

(3) Tall buildings' aeroelastic behavior is influenced by both the wind-structure interaction mechanism and the structural torsional/lateral mode coupling effect.

Acknowledgement
The authors wish to express their appreciation to the National Science Council of the Republic of China for partial financial support under Contract No. NSC90-2211-E032-010

REFERENCES

1. Marukawa, H., N. Kato, K. Fujii & Y. Tamura, Experimental evaluation of aerodynamics, *Journal of Wind Engineering and Industrial Aerodynamics,* (59) 177-190.
2. C.M. Cheng, P.C. Lu, and M.S. Tsai, Acrosswind aerodynamic damping of isolated square shaped buildings", *Journal of Wind Engineering and Industrial Aerodynamics*, 90 (2002) 1743-1756.
3. B.J. Vickery and A. Steckley, Aerodynamic damping and vortex excitation on an oscillating prism in turbulent shear flow, *Journal of Wind Engineering and Industrial Aerodynamics,* 49 (1993) 121-140.
4. R.H. Chen, C.M. Cheng, and P.C. Lu, Wind-structure interaction of a high-rise building in boundary later flows, *Journal of the Chinese Institute of Civil and Hydraulic Engineering*, Vol. 9, No. 2 (1997) 271-280. (in Chinese)
5. J. Katagiri, T. Ohkuma, and H. Marikawa, Motion–induced wind forces acting on rextangular high-rise buildings with side ratio of 2, *Journal of Wind Engineering and Industrial Aerodynamics,* 89 (2001) 1421-1432.
6. A. Kareem, Lateral-torsional motion of tall buildings to wind loads, *Journal. of Structural Engineering,* ASCE. 111(11) (1985) 2479-2496.
7. E. Safak and D.A Foutch, Coupled vibrations of rectangular buildings subjected to normally incident random wind loads, *Journal of Wind Engineering and Industrial Aerodynamics,* 26 (1987) 129-148.
8. L.Y. Xu, K.C.S. Kwok and B. Samali, torsion response and vibration suppression of wind –excited buildings, *Journal of Wind Engineering and Industrial Aerodynamics*, Vol.41-44 (1992) 1997-2008.
9. C.M. Cheng, P.C. Lu, and H.Y. Lo, Acrosswind responses of square shaped high-rise buildings with eccentricities, *Wind Engineering into the 21st Century*, Proceedings of the Tenth International Conference on Wind Engineering, Copenhagen/Denmark, 1999, pp. 631-636.
10. J. Katagiri, H. Marukawa, A. Katsumura, and K. Fujii, Effects of structural damping and eccentricity on wind responses of high-rise buildings, *Journal of Wind Engineering and Industrial Aerodynamics,* 74-76, (1998) 731-740.
11. S. Thepmongkorn and K.C.S. Kwok, , 2002, "Wind-induced responses of tall buildings experiencing complex motion", *Journal of Wind Engineering and Industrial Aerodynamics*, 90 (2002) 515-526.